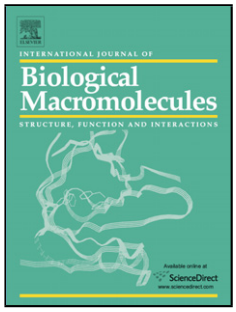

Title: Chitosan-ZnO/Polyanilne nanocomposite modified glassy carbon electrode for selective detection of dopamine

Author: K. Pandiselvi S. Thambidurai

PII: S0141-8130(14)00181-0
DOI: http://dx.doi.org/doi:10.1016/j.ijbiomac.2014.03.028
Reference: BIOMAC 4240

To appear in: *International Journal of Biological Macromolecules*

Received date: 2-12-2013
Revised date: 17-3-2014
Accepted date: 19-3-2014

Please cite this article as: K. Pandiselvi, S. Thambidurai, Chitosan-ZnO/Polyanilne nanocomposite modified glassy carbon electrode for selective detection of dopamine, *International Journal of Biological Macromolecules* (2014), http://dx.doi.org/10.1016/j.ijbiomac.2014.03.028

Chitosan-ZnO/Polyanilne nanocomposite modified glassy carbon electrode for selective detection of dopamine

K.Pandiselvi, S.Thambidurai*

Department of Industrial Chemistry, School of Chemical Sciences, Alagappa University, Karaikudi 630003, Tamil Nadu, India.

*Corresponding author Tel/Fax: +91 4565 228836

Email: sthambi01@yahoo.co.in (S.Thambidurai)

ABSTRACT

In this study, inorganic-organic redox mediators of CS-ZnO/PANI nanocomposite were synthesized by simple precipitation and chemical polymerization approach in the presence of chitosan (CS), $ZnCl_2$, polyaniline (PANI) and ammonium peroxydisulfate (APS) as an initiator. The formation of ZnO nanoparticles onto CS-PANI matrix was confirmed by SEM, TEM, Raman and FT-IR spectroscopies. Cyclic voltammetry and electrochemical impedance spectroscopy (EIS) were used to evaluate the electrochemical performance of the CS-ZnO/PANI. The obtained $CS_{\mathbf{0.12}}$-$ZC_{\mathbf{2.5}}$/PANI nanocomposite modified electrode has been successfully developed for selective determination of dopamine (DA) in the presence of ascorbic acid (AsA) in 0.2 M phosphate buffer solution pH 7.0. The electrochemical oxidation signals of AsA and DA are well separated into two distinct peak potential separation of 303 mV in DPV studies, which is large enough to allow the determination of one in the presence of the other. A linear response for DA concentrations range from 20 x 10^{-5} to 180 x 10^{-5}, in the presence of 140 x 10^{-5} AsA, with sensitivity of 0.013 μA/μM and a detection limit of 0.21 μM, have been obtained. Moreover, $CS_{\mathbf{0.12}}$-$ZC_{\mathbf{2.5}}$/PANI modified glassy carbon electrode (GCE) had good stability and antifouling properties. The proposed biosensor offers promise for simple and cost-effective analysis of bio-molecules.

Keywords

Chitosan, Zinc chloride, SEM, Differential Pulse Voltammetry, Dopamine.

1. Introduction

Development of sensitive, selective, reliable and low-cost as say methods for the detection of physiologically-related species in biological matrixes has attracted considerable attention in recent years, and how to construct fast, simple and selective determination of electro-active analytes in a mixed systems is still a challenges for analytical researchers. DA is one of the excitatory neurotransmitters that play an important role in the functioning of the central nervous system as well as in the cardiovascular, renal and hormonal systems [1]. An excess or deficiency of DA can result in brain disorders such as schizophrenia and Parkinson's disease and neuroendocrine disorder [2-3]. However, one of the major problems encountered in the electrochemical determination of DA is the intervention of AsA, which has similar structure and oxidation potential close to DA. Being AsA exists as an anion while DA exists as a cation. Therefore, AsA interacts with DA strongly. These facts can largely affect the determination of DA in the presence of AsA [4]. To solve this issue, many researchers have been developed to modify the various electrode materials applied for selective detection of DA in the presence of AsA [5-10].

Among the various methods of biomolecule immobilization for the construction of metal oxide-based composites, a technique based on electrostatic interactions has attracted significant attention because of its procedural simplicity [11]. Biocompatibility is an important prerequisite for the construction of a biosensor. A bio-compatible matrix may prevent the deactivation of biomolecules. In this context, the combination of metal oxide nanoparticles (ZnO) dispersed in chitosan (CS) has been used for immobilization of desired biomolecules [12-13] for

improvement of human igc [14], H_2O_2 and colorectal cancer DNA [15-16]. CS is an abundant natural biopolymer with excellent film forming abilities, biocompatility, nontoxicity, good water permeability, high mechanical strength [17] and susceptible to chemical modification due to the presence of reactive hydroxyl and amino functional groups. On the other hand zinc oxide (ZnO) is one of the important semiconductors in II–VI group, has been attracting considerable interest because of its combined properties of high surface area, nontoxicity, good biocompatibility, easy fabrication, plentiful oxygen vacancies, optical transparency, chemical and photochemical stability, and good electrocatalytic activity [18-20].

Furthermore, CS along with polyaniline (PANI) a conducting polymer provides a suitable matrix for covalent immobilization and stabilization condition for the biomolecules [21]. PANI is one of the most attractive conducting polymers because of its high conductivity, ease of preparation, good environmental stability and extensive applications, such as electrochemical analysis, catalysis, electronic devices and biosensors. For example, glucose can be selectively detected in the presence of more interference at electrodes modified with CS/PANI [22], substituted PANI/CS composite [23], CS-polypyrrole [24] and cDNA by CS-co-PANI [25]. It was also reported that detection of cretinine and sarcosine oxidase by Fe_3O_4/CS-g-PANI [26] and ZnO/CS/c-MWCNT/PANI composites [27]. But, to the best of our knowledge, it has not been reported that multi-component composite comprising of CS, $ZnCl_2$ and PANI (CS-ZnO/PANI) based composite film for the determination of DA.

In the present investigation, a non-enzymatic and without using any specific reagent for the selective electrochemical determination of DA was found in the CS-ZnO/PANI/GCE nanocomposite and the results showed that high sensitivity, fast response (>2 s) and low detection limit. Also, the separation between the oxidation peak potential of AsA and DA was

large enough for the selective determination of DA in the presence of high concentration of AsA. Especially, the preparation and modification of CS-ZnO/PANI/GCE nanocomposite film was quite simple and stable. This strategy offers an effective way for the selective detection of DA.

2. Materials and methods

2.1. Reagents and materials

Chitosan with 90% deacetylation and an average molecular weight of 180 kDa was obtained from M/s South India Sea Foods, kochi (India), Monomer aniline (SRL) was purified by double distillation before use. Dopamine hydrochloride (98%), l-ascorbic acid (99%) were obtained from Spectrochem Pvt. Ltd, Zinc(II) chloride hexahydrate ($ZnCl_2$. $6H_2O$), ammonium peroxydisulfate (APS), hydrochloric acid (HCl) (35% concentrated), Disodium phosphate (Na_2HPO_4), monosodium phosphate (NaH_2PO_4) and N, N-Dimethylformamide (DMF) were purchased from Sigma-Aldrich. The supporting electrolyte used for all experiments was phosphate buffer solution (PBS, 0.2 M, pH 7.0), which was prepared using 0.1 M Na_2HPO_4 and NaH_2PO_4 solutions were kept at 4°C before use. All other chemicals were of analytical grade and were used as received. All solutions were prepared with double-distilled water and high purity N_2 was applied for deaeration.

2.2. Synthesis of CS-ZnO/PANI nanocomposites

The CS-ZnO/PANI nanocomposites were prepared by chemical co-precipitation method as reported previously [28]. Following this method, the preparation of CS-ZnO/PANI ternary nanocomposites with addition of 2.5, 5% $ZnCl_2$ were designated as CS-$ZC_{2.5}$/PANI, CS-ZC_5/PANI and decreasing the CS content 0.12 g were designated as $CS_{0.12}$-$ZC_{2.5}$/PANI

respectively. For comparison purpose, chitosan-polyaniline binary nanocomposite under the same procedure except that $ZnCl_2$ was not added which is denoted as CS-PANI.

2.3. Fabrication of CS-ZnO/PANI nanocomposites modified electrode

Before modification, the bare GCE (3 mm in diameter) was polished to a mirror like surface with alumina slurry (0.5 μM followed by 0.05 μM). After removal of the trace alumina from the electrode surface, rinsed with ultrapure water and acetone in an ultrasonic bath and allowed to dry at room temperature. Then GCE was electrochemically activated by using potential cycling in the range of -0.5 to 1.0 V in 0.5 M H_2SO_4 solution at a scan rate of 50 mVs^{-1} [29]. The working electrode was prepared by dissolving 5 mg of CS-ZnO/PANI nanocomposites in 5 mL of N, N-Dimethylformamide (DMF), sonicated for 20 min to form a suspension ink. Then 5 μL of 5 mg mL^{-1} CS-ZnO/PANI suspension was spread evenly onto the surface of pretreated GCE with a micro syringe which was dried for 30 min at room temperature; the solvent evaporated and left the CS-ZnO/PANI on the electrode surface. Finally, the CS-ZnO/PANI modified GCE was thoroughly rinsed with double-distilled water. For comparison, CS-PANI/GCE was also prepared by the similar method.

2.4. Characterization and electrochemical measurements

The electrochemical experiment was conducted in a conventional three-electrode system using a modified GCE as the working electrode, a platinum foil as the counter electrode and a saturated calomel electrode (SCE) as the reference electrode. All electrochemical measurements of cyclic voltammetry (CV), Differential pulse voltammetry (DPV) and Electrochemical impedance spectroscopy (EIS) were performed on a AUTOLAB CHI 1102A workstation. All measurements were performed at room temperature. The surface studies of CS-ZnO/PANI and CS-PANI modified electrodes were characterized by scanning electron microscopy (HRSEM-

FEI Quanta FEG 200) and transmission electron microscopy (HRTEM-CM200). Raman spectra were recorded at 1 cm^{-1} resolution using Renishaw Raman System-Model 1000 spectrometer with laser excitation (785 nm). Fourier transform infrared (FT-IR) spectra were measured using (SHIMADZU spectrometer).

3. Results and discussion

3.1. Morphology of CS-PANI and CS-ZnO/PANI nanocomposites

The surface morphologies of CS-PANI, CS-$ZC_{2.5}$/PANI, CS-ZC_5/PANI and $CS_{0.12}$-$ZC_{2.5}$/PANI modified electrodes were characterized by FE-SEM and typical results are shown in Fig. 1.

Position of Figure 1

It can be observed that CS-PANI matrix have a granular porous morphology with minimum aggregation (Fig. 1a), whereas the CS-ZnO/PANI nanocomposites has wrinkled sheet-like structure attributed to the homogeneous dispersion of ZnO nanoparticles in CS-PANI matrix (Fig. 1b-d). From the images, $CS_{0.12}$-$ZC_{2.5}$/PANI nanocomposite exhibits a much more sheets in comparison with CS-$ZC_{2.5}$/PANI and CS-ZC_5/PANI; this would be of benefit to the sensor performance because the well-dispersed hybrid composites were electrochemically accessible [30]. The microstructure of the CS-PANI and CS-ZnO/PANI modified electrodes was further investigated by TEM and the corresponding images were displayed in Fig. 2.

Position of Figure 2

It was found that the morphology of the CS-PANI changed to a core-shell structure and CS-ZnO/PANI nanocomposites reveal spherical shaped aggregate structure. The diameter of the CS-

PANI was varied from 400 to 450 nm and a CS-ZnO/PANI was 100-200 nm. From the TEM images, the morphology of $CS_{0.12}$-$ZC_{2.5}$/PANI show less particle aggregation with homogeneous dispersion of ZnO nanorods, which means effects of CS and $ZnCl_2$ in the polymer composites, has effectively improved the particles morphology. The results also suggest that higher amount of CS and $ZnCl_2$, while the phase evolution does not significantly alters the general morphology of the polymer composites. In addition the selected area electron diffraction (SAED) pattern is an extremely useful technique that enables to ascertain the structural information of the as-prepared materials. The SAED pattern of representative $CS_{0.12}$-$ZC_{2.5}$/PANI nanocomposite in (inset Fig. 2d) shows a different planes of hexagonal wurtzite-type ZnO, and the spacing of about 0.281, 0.260 and 0.247 nm which correspond to the planes of (1 0 0), (1 0 2), (1 0 1) hexagonal wurtzite-type ZnO crystal [31].

3.2. Raman and FT-IR spectroscopy

The formation of CS-ZnO/PANI nanocomposites was confirmed by Raman and FTIR spectroscopy. Fig. 3a presents the Raman spectra of CS-PANI and $CS_{0.12}$-$ZC_{2.5}$/PANI nanocomposites.

Position of Figure 3

The spectrum of CS-PANI show prominent peaks at 1338 and 1563 cm^{-1} corresponding to C=C and C=N stretching vibrations of benzenoid and quionoid units in oxidation states of PANI, respectively [32]. The dominating and less intense peaks observed at 783 cm^{-1} C-H wag out-of-plane of the benzenoid ring and 652 cm^{-1} quinoid deformation [33], which is probably with the interaction of CS with PANI chains [34], or with the overlapping CS and PANI bands. For the $CS_{0.12}$-$ZC_{2.5}$/PANI nanocomposites, C-H bending of the quinoid ring at 1161 cm^{-1}, C-N

stretching vibrations at 1220 cm^{-1}, and C=C (benzenoid), C=N (quinoid) stretching vibrations at 1480, 1586 cm^{-1} are observed, revealing the presence of PANI in oxidation states. Moreover, the peak at 416 cm^{-1} corresponds to the optical phonon E_2 (high) mode of wurtzite hexagonal phase ZnO [35]. Compared with CS-PANI, the spectrum of the $CS_{\mathbf{0.12}}$-$ZC_{\mathbf{2.5}}$/PANI shows the Raman modes slightly shifted to higher wave numbers and the decrease in relative intensity of bands for benzene and quinone stretching vibrations, attributed to the formation of hydrogen bonding between $ZnCl_2$ and the N-H group of the polymer on the surface of the Zn (OH) particles [36].

The structural information of CS-PANI and $CS_{0.12}$-$ZC_{2.5}$/PANI was further confirmed by FTIR spectroscopy and presented in Fig. 3B. The spectrum of CS-PANI contains the locations of all characteristics absorption peaks of PANI and CS are in good agreement with the previous reported literature [37]. The main characteristic absorption peaks of CS-PANI at 1579, 1437, 1305 and 1117 cm^{-1} were attributed respectively, to C=C stretching of the quinoid (N=Q=N ring), C=C stretching of the benzanoid (N-B-N ring), C-N stretching of the secondary aromatic amine and N=Q=N stretching of in-plane bending vibrations. The broadening of bands between 2929 and 3429 cm^{-1} is due to H-bonding interaction between PANI and CS [34]. The presence of ZnO nanoparticles in $CS_{0.12}$-$ZC_{2.5}$/PANI leads to the shift of some peaks and changes of relative intensity. In particular, the peaks at 1579, 1437 and 1391 cm^{-1} that shifted to higher wave numbers of 1633, 1506 and 1391 cm^{-1} which indicates that amine (-NH-) and imine (-N=) nitrogen atoms bonding with Zn^{2+} via either protonation or complexation [38]. Moreover, the intensity of the band around 1115 cm^{-1} was much stronger and the broad beak appeared at 436 cm^{-1} is corresponding to O-Zn-O stretching vibration [39]. These results are suggested that existence of interactions between the CS-PANI and ZnO nanoparticles and consistent with Raman spectroscopy.

3.3. Electrochemical characterization of the composite electrodes

The electrochemical behaviors of different modified electrodes were investigated in 0.2 M/L PBS (pH 7.0) containing 1.0 mM $Fe(CN)_6^{3-/4-}$ solution with cyclic voltammetry, as shown in Fig. 4.

Position of Figure 4

Well-defined cyclic voltammogram and characteristics of a diffusion-controlled redox process were observed at the bare GCE (Fig. 4a). After the electrode was modified with CS-PANI, the redox peaks increased little, which could be attributed to the larger effective surface area and also good electric conductivity of PANI [24, 40]. For CS-ZnO/PANI/GCE (Fig. 4c-e), the peak currents increased more and ΔEp became smaller compared with the CS-PANI modified electrode. The results demonstrated that the surface charged ZnO nanoparticles interact with the cationic biopolymer matrix of CS and synthetic polymer of PANI via electrostatic interactions and hydrogen bonding with NH_2/OH groups to form a hybrid bionanocomposite [41, 28]. In other words the anodic peak potential slightly shifted towards positive side with increase in current and cathodic peak potential shifted to reverse direction in the presence of CS-$ZC_{2.5}$/PANI.

The CS-$ZC_{2.5}$/PANI nanocomposite exhibits higher peak current than the CS-PANI matrix at neutral pH environment, which indicate that CS-$ZC_{2.5}$/PANI, have larger effective surface area than CS-PANI matrix could provide a conducting path through the composite matrix for faster kinetics. Hence, the ZnO-nanoparticles, acting as electron transfer mediator could help increase the sensitivity of the biosensor and was similar to results from ZnO-NPs/CHIT/c-

MWCNT/PANI and Fe_3O_4-NPs/CHIT-g-PANI hybrid systems in neutral environment [26, 27] In addition of 5% $ZnCl_2$ in CS-ZC_5/PANI modified electrode (curve d) obviously decreased the electrode conductivity which indicates higher amount of ZnO nanoparticles could prevent the PANI oxidation. Similar results have been obtained in the previous report [28].

When the concentration of CS was reduced to 0.12 g in $CS_{0.12}$-$ZC_{2.5}$/PANI was used to modify the electrode the largest peak current value (Fig. 4e) in comparison with the other four electrodes, implying the excess amount of carboxy methyl cellulose will prevent the transfer of electrons and gathering charge [42]. Therefore, the CS concentration of 0.12 g was chosen in this work.

Cyclic voltammograms of $CS_{0.12}$-$ZC_{2.5}$/PANI modified GCE with different scan rates are shown in Fig. 5.

Position of Figure 5

With increasing scan rate, the anodic and cathodic peak current values increased linearly, while the peak-to-peak separation (ΔEp) also increased. The plot of the oxidation and reduction peak currents against the scan rates (correlation coefficient values of 0.998 and 0.998 for anodic and cathodic peaks, respectively in Fig. 5, inset), which suggests that the electrochemical process is a diffusion-controlled electron transfer process rather than surface controlled at these scan rates [43].

Electrochemical impedance spectroscopy (EIS), as one of the electrochemical technologies, has been proven to be one of the most powerful tools for interfacial investigation. Fig. 6 shows Nyquist plots of the EIS of bare GCE (curve a), CS-PANI/GCE (curve b) and $CS_{0.12}$-$ZC_{2.5}$/PANI modified GCE (curve c), respectively, which were obtained in a solution of

0.2 M/L PBS (pH 7.0) containing 1.0 mM $Fe(CN)_6^{3-/4-}$ with the frequencies ranging from 10 kHz to 0.1 Hz at 5 mV amplitude.

Position of Figure 6

The Nyquist plot consisted of two steps includes a semicircle and linear portion, with the former at higher frequencies corresponding to the electron transfer limited process and the latter at lower frequencies corresponding to the diffusion process. The electron transfer resistance (Rct) at electrode surface is equal to the semicircle diameter, which can be used to describe the interface properties of the electrode [44]. The bare GCE exhibited an almost straight line (curve a), indicating a diffusion limiting step of the electrochemical process. After assembling of CS-PANI composite on the electrode surface, the Rct was found to be 1575Ω (curve b), revealing that the use of CS-PANI composite inhibited the interfacial electron transfer and enhanced the electron transfer resistances.

As compared with CS-PANI, the Rct value of the $CS_{0.12}$-$ZC_{2.5}$/PANI/GCE (curve c) reduced obviously, indicating the presence of ZnO nanoparticles in the composite playing an important role in accelerating the transfer of the electrons, thus decreasing the resistance of the $CS_{0.12}$-$ZC_{2.5}$/PANI nanocomposite to $Fe(CN)_6^{3-/4-}$. These results obtained from EIS were in agreement with the results obtained from the CVs.

3.4. Cyclic voltammetric behavior of AsA at $CS_{0.12}$-$ZC_{2.5}$/PANI/GCE

Fig. 7A gives the CV responses of the bare GCE and $CS_{0.12}$-$ZC_{2.5}$/PANI modified GCE in 0.2 M PBS (pH 7.0) in the absence and presence of 0.5 mM AsA with a scan rate at 50 mV/s. When there is no AsA in PBS, almost no oxidation peaks appear in the CV (curve a). But when the concentration of AsA was 0.5 mM in PBS, an irreversible oxidation peak of the bare GCE

was observed at 0.275 V. Under the identical conditions, the $CS_{0.12}$-$ZC_{2.5}$/PANI/GCE obviously increased a fast electron transfer process to AsA.

Position of Figure 7

A well-defined oxidation wave of AsA at the anodic peak potential of 0.191 V was observed, which lowered the anodic overpotential of AsA by about 0.275 V. The greatly enhanced current and the potential shift towards negative potential values observed for AsA oxidation can be ascribed to the electrostatic interaction of ascorbate anions with the polarons by $CS_{0.12}$-$ZC_{2.5}$/PANI nanocomposite. It is well known that conducting polymers can act as redox mediators and the electrocatalytic activity arises from the formation of polarons, which is of positive charges on the polymer backbone. Therefore, the oxidation of AsA is facilitated at $CS_{0.12}$-$ZC_{2.5}$/PANI modified electrode by the negative charge of the molecule. The CV responses of the $CS_{0.12}$-$ZC_{2.5}$/PANI modified GCE in 0.2 M PBS with different concentrations of AsA (1-5 mM) is presented in Fig. 7B. The oxidation current of AsA increased with increasing AsA concentration, indicate that the $CS_{0.12}$-$ZC_{2.5}$/PANI modified GCE effectively catalyzes the oxidation of AsA.

3.5. Catalytic oxidation of DA at the $CS_{0.12}$-PANI/$ZC_{2.5}$ modified electrode

Fig. 8 shows the cyclic voltammograms of 0.1 mM DA in PBS (pH 7.0) at a bare GCE and a $CS_{0.12}$-$ZC_{2.5}$/PANI/GCE. At a bare GCE, an anodic peak was observed with an oxidation peak potential of 0.224 V, a reduction peak potential of 0.067 V (curve a), and a peak separation (ΔEp) of 157 mV. Under the same conditions, the $CS_{0.12}$-$ZC_{2.5}$/PANI/GCE gave highly enhanced redox peak currents and a more reversible electron transfer process to DA.

Position of Figure 8

A well-defined redox wave of DA was observed, with anodic and cathodic peak potentials of 0.197 and 0.079 V, respectively (curve b). The separation of peak potentials (ΔEp) at the $CS_{0.12}$-$ZC_{2.5}$/PANI/GCE was 118 mV. The improved reversibility could be due to the π-π* interactions between the benzene ring of DA and PANI. On the other hand, the presence of the negatively charged hydroxide ions in the polymer matrix could influences the oxidation of DA, which is consistent with a literature report for a similar behavior observed at ordered mesoporous carbon (OMC) modified electrode under alkali conditions [45]. Therefore, the electrochemical response of the modified electrode towards both analytes can be considered as a result of a synergistic behavior of the organic and inorganic components of the composite material. This suggests an efficient catalytic activity toward DA at the $CS_{0.12}$-$ZC_{2.5}$/PANI nanocomposite. The current response of DA with different concentration at $CS_{0.12}$-$ZC_{2.5}$/PANI/GCE is also investigated. As shown in Fig. 8B, the electrocatalytic peak current increase by increasing the concentration of DA (0.1-0.5 mM) in PBS, indicate that this new modified electrode has higher electrocatalytic activity toward DA oxidation.

3.6. Cyclic voltammetric behavior of AsA and DA at $CS_{0.12}$-$ZC_{2.5}$/PANI modified GCE

Fig. 9 depicts the cyclic voltammetric response of the bare GCE and $CS_{0.12}$-$ZC_{2.5}$/PANI modified GCE in 0.2 M PBS containing 1 mM AsA and DA. As shown in Fig. 9a, bare GCE obtained for the mixture of AsA and DA exhibits only one anodic peak. It is believed that oxidized DA acts as a catalyst for oxidation of AsA, which is also one of the reasons why only one oxidation peak with great peak current was obtained for AsA and DA mixture. These observations clearly indicated that the existence of AsA had seriously interfered with the determination of dopamine at bare GC electrode [46-48].

Position of Figure 9

In Fig. 9b $CS_{0.12}$-$ZC_{2.5}$/PANI modified GCE shows the DA oxidation produces an anodic wave at 0.376 V, while the AsA oxidation occurs at 0.048 V that is a peak potential separation of ca. 168 mV was obtained. The large peak potential separation obtained at the modified electrode is attributed to the following reasons: i) PANI is π-rich in nature, the π-π interaction between phenyl structure of DA and PANI makes the easy arrival of DA molecules to the surface of modified electrode [49]. ii) Secondly, although the π-π interaction between penta-heterocycle of AsA and PANI is week, the presence of negatively charged AsA in PBS (pH 7.0) due to the charge characteristic of AsA (pKa = 4.10). iii) At physiological pH, DA had a positive charge, while AsA was negative. The polymer nanocomposite is a cation exchange or adsorption capabilities, and the negatively charged hydroxide groups form a selective polymeric net. Also the oxide particles may be served as the mediator for the oxidation of DA and improve the electro catalytic ability [50].

Moreover, it was observed that the peak current of DA is higher than AsA on $CS_{0.12}$-$ZC_{2.5}$/PANI/GCE, which was sufficient enough for the determination of DA in the presence of AsA and well, avoids the co-oxidation of AsA and DA at the same potential window [51-53]. According to the above discussion, the mechanism of DA oxidation at this modified electrode could be described as in Scheme 1. During oxidation of DA on CS-ZnO/PANIGCE, DA undergoes a two-electron oxidation process resulting in dopamine-o-quinone (DOQ). Similar behaviors have been proposed for the determination of DA on ZnO/redox mediator and MnOOH nanobelt modified electrodes [54-55].

Position of Scheme 1

In view of sensing experiments, many reports have demonstrated that the pH value lower than neutral is favorable for higher sensitivity and higher selectivity. However, in order to maintain the physiological environment, pH 7.0 was chosen in our present study.

3.7. The selective determination of DA in the presence of AsA

The main aim of the present investigation is to selectively detect the concentration of DA in the presence of AsA. Differential pulse voltammetry has a much higher current sensitivity and better resolution than cyclic voltammetry and hence used to determine the selective electro-oxidation of DA in the presence of AsA. Fig. 10A shows the DPV curves for the bare GCE and modified GCE recorded during the voltammetric determination of 0.1 mM DA in the presence of an excess of 1 mM AsA at the scan rate of 50 mV/s with pulse amplitude of 50 mV and pulse width of 10ms in 0.2 M PBS.

Position of Figure 10

DA oxidation produces an anodic wave at 0.346 V, while the AsA oxidation occurs at -0.043 V that is a peak potential separation of ca. 303 mV, which was large enough for the determination of DA in the presence of AsA [56]. The $CS_{\mathbf{0.12}}$-$ZC_{\mathbf{2.5}}$/PANI/GCE showed a strong electrocatalytic activity towards the oxidation of DA, what's more, the current responses of 0.1 mM DA higher than 1 mM AsA. Due to the strong electric repelling between AsA and $CS_{\mathbf{0.12}}$-$ZC_{\mathbf{2.5}}$/PANI/GCE, the electrochemical oxidation of AsA was inhibited seriously. Thus, only a low current response could be seen. It is also reported that hydrophobicity of the polymer matrix is one of the important factors that is responsible for the selective DA receptor ligand bonding [57]. Because DA is more hydrophobic than AsA and it is likely that DA interact with reduced regions of PANI

through hydrophobic-hydrophobic interactions, whereas AsA does not [1]. Hence, the determination of DA could be achieved even in the presence of high concentration of AsA.

Fig. 10B shows the DPV curves for the oxidation of various concentration of DA in presence of 140 μM AsA in PBS (pH 7.0) at $CS_{0.12}$-$ZC_{2.5}$/PANI/GCE. The peak current for DA increased with the increase of the concentration. As shown in inset (Fig. 10B), plot of the peak current as a function of concentration gave a linear line in the wide range from 20 x 10^{-5} mol L^{-1} to 180 x 10^{-3} mol L^{-1}, and the linear regression equation was expressed as ip (μA) = 0.013C(μM) + 0.756, with a correlation coefficient of 0.997.

Moreover, the peak intensity and position of AsA did not change with the variation of the concentration of DA in the above mentioned range, signifying that AsA could not interfere to the sensitivity of the DA at $CS_{0.12}$-$ZC_{2.5}$/PANI/GCE and the selective detection of DA is possible from binary DA-AsA mixture at the modified $CS_{0.12}$-$ZC_{2.5}$/PANI/GCE. Furthermore, the detection limit was estimated to be 2.1 x 10^{-7} M L^{-1} at a signal-to-noise ratio of 3, which is calculated using 3sB/S, where sB is the standard deviation obtained from 10 blank measurements, and S is the sensitivity of the measurement (slop of the calibration curve) [58]. Table 1 compares detection limits and linear concentration ranges of the proposed biosensor for the determination of DA with other DA biosensors.

Position of Table 1

To our knowledge, these analytical parameters are the best reported values for DA determination in physiological pH and when using a simple, cheap, and reproducible sensor without using any specific reagent. The optimum current response was obtained at pH 7.0 which is similar to earlier reported biosensor based ZnO based polymer composites [55].

3.8. Reproducibility and stability

In order to study the reproducibility of the biosensor and reliability of fabrication procedure, seven replicate $CS_{0.12}$-$ZC_{2.5}$/PANI/GCE were prepared independently. Differential pulse voltammograms of $CS_{0.12}$-$ZC_{2.5}$/PANI/GCE were recorded in 0.2 M PBS (pH 7.0) containing 0.01mM DA, the average currents were 0.219 μA with RSD of ±0.09% (n=7). It indicated that the modified electrode has a good reproducibility. To test the stability of the $CS_{0.12}$-$ZC_{2.5}$/PANI was investigated by keeping the modified electrode at room temperature when not in use. After 15 days of storage, the biosensor retained about 91% of its initial response.

3.9. Effect of interferences

In order to evaluate the selectivity of the proposed biosensor, the influences of AsA and glucose on the determination of DA was studied. When considering the blood as a sample for the detection of dopamine, glucose is an important interfering agent [64]. The concentration of interferences compounds were chosen to be 20 times higher than the level of DA. Fig. 11 shows DPV curves of $CS_{0.12}$-$ZC_{2.5}$/PANI/GCE in 0.2 M PBS (pH 7.0) containing 0.1mM AsA and glucose with different concentration (0.001-0.005 mM) of DA.

Position of Figure 11

The oxidation peak current of DA increases linearly with the increase of DA concentration. It can be observed that 20 times larger addition of the AsA, much constant detected peak of AsA and no characteristic peaks of glucose, compared to that of DA (curve a-e). Moreover, the peak intensity and position of AsA did not change with the variation of the concentration of DA, signifying that selective detection of DA on $CS_{0.12}$-$ZC_{2.5}$/PAN/GCE can still be achieved in the solution with interfering agents.

3.10. Determination of DA in real samples

Analytical applicability of the modified electrode, we carried out DPV studies of dopamine hydrochloride injections. The dopamine injection (specified content of DA is 50 mg ml^{-1} was diluted to 250 mL with water, and then different amounts of dopamine were transferred into series of 20 mL volumetric flasks and diluted to a mark with a phosphate buffer of pH 7.0. The resulted solutions were placed in the cell and analytical responses were recorded. The obtained results are presented in Table. 2.

Position of Table 2

The recovered ratio indicates that determination of DA using the proposed method is effective and can be applied for the detection of DA in commercial samples.

Conclusions

In summary, environment friendly CS-ZnO/PANI nanocomposites were successfully prepared by co-precipitation and chemical oxidative polymerization of aniline with CS-ZnO composite using APS as an oxidant. $CS_{0.12}$-$ZC_{2.5}$/PANI modified GCE was fabricated for the electrocatalytic oxidation of DA in the presence of AsA in physiological solution. It was found that the oxidation peaks of AsA and DA shifted towards more negative and positive potential when compared to bare GCE. The modified electrode has low detection limit, wide linear dynamic range and good antifouling ability. Moreover, they had inhibitive effect on oxidation of AsA. Thus, the determination of DA can be conducted in the presence of large amounts of AsA. The proposed method has also been applied for detecting dopamine in real sample analysis with satisfactory results. Such a novel sensor may be used as a potential sensing for detection of DA under coexistence of AsA in vivo.

Acknowledgement

The authors would like to thank the University Grant Commission, New Delhi, for providing financial assistance to the first author under Rajiv Gandhi National Fellowship (RGNF).

References

[1] S. Senthil Kumar, J. Mathiyarasu, K. Lakshminarasimha Phani, Exploration of synergism between a polymer matrix and gold nanoparticles for selective determination of dopamine, J. Electroanal. Chem. 578 (2005) 95–103.

[2] T. Luczak, Preparation and characterization of the dopamine film electrochemically deposited on a gold template and its applications for dopamine sensing in aqueous solution, Electrochim. Acta 53 (2008) 5725-5731.

[3] X.Q. Lin, L. Zhang, Simultaneous determination of dopamine and ascorbic acid at glutamic acid modified graphite electrode, Anal. Lett. 34 (2001) 1585-1601.

[4] X. Zhou, N. Zheng, S.H. Hou, X.J. Li, Z.B. Yuan, Selective determination of dopamine in the presence of ascorbic acid at a multi-wall carbon nanotube-poly(3,5-dihydroxy benzoic acid) film modified electrode, J. Electroanal. Chem. 642 (2010) 31-34.

[5] Q. Liu, X. Zhu, Z. Huo, X. He, Y. Liang, M. Xu, Electrochemical determination of dopamine in the presence of ascorbic acid using PVP/graphene modified electrodes, Talanta 97 (2012) 557-562.

[6**]** M.H. Mashhadizadeh, T. Yousefia, A.N. Golikand, A nickel hexacyanoferrate and poly(1-naphthol) hybrid film modified electrode used in the selective electroanalysis of dopamine, Electrochim. Acta 59 (2012) 321– 328.

[7] D.P. Quan, D.P. Tuyen, T. D. Lam, P.T.N. Trama, N.H. Binh, Electrochemically selective determination of dopamine in the presence of ascorbic and uric acids on the surface of the modified Nafion/single wall carbon nanotube/poly(3-methylthiophene) glassy carbon electrodes, Colloids Surf. B 88 (2011) 764-770.

[8] M. Mallesha, R. Manjunatha, C. Nethravathi, G.S. Suresh, M. Rajamathi, J.S. Melo, T.V. Venkatesha, Functionalized-graphene modified graphite electrode for the selective determination of dopamine in presence of uric acid and ascorbic acid, Bioelectrochemistry 81 (2011) 104–108.

[9] Y. Li, X. Liu, X. Zeng, X. Liu, B. Konga, W. Wei, S. Luo, Selective and sensitive detection of dopamine in the presence of ascorbic acid by molecular sieve/ionic liquids composite electrode, Electrochim. Acta 56 (2011) 2730–2734.

[10] W. Yan, X. Feng, X. Chen, X. Li, J.J. Zhu, A selective dopamine biosensor based on AgCl@polyaniline core–shell nanocomposites, Bioelectrochemistry 72 (2008) 21–27.

[11] X. Yi, J. Huang-Xian, C. Hong-Yuan, Direct electrochemistry of HRP immobilized an Au colloid-cysteamine monolayer modified gold electrode, Anal Biochem. 278 (2000) 22-28.

[12] S.P. Singh, S.K. Arya, M.K. Pandey, B.D. Malhotra, S. Saha, K. Sreenivas, V. Gupta, Cholesterol biosensor based on rf sputtered zinc oxide nanoporous thin film, Appl. Phys. Lett. 99 (2006) 123902.

[13] A. Wei, X.W. Sun, J.X. Wang, Y. Lei, X.P. Cai, C.M. Li, Z.L. Dong, W. Huang, Enzymatic glucose biosensor based on ZnO nanorod array grown by hydrothermal decomposition, Appl. Phys. Lett. 99 (2006) 123902.

[14] Z. Wang, Y. Yang, Z. Li, J. Gong, G. Shen, R. Yu, Organic–inorganic matrix for electrochemical immunoassay: Detection of human IgG based on ZnO/chitosan composite**,** Talanta 69 (2006) 686-690.

[15] Y.Q. Miao, S.W. Tan, Amperometric hydrogen peroxide biosensor based on immobilization of peroxidase in chitosan matrix crosslinked with glutaraldehyde, Analyst 125 (2000) 1591–1594.

[16] K.J. Feng, Y.H. Yang, Z.J. Wang, J.H. Jiang, G.L. Shen, R.Q. Yu, A nano-porous CeO_2/Chitosan composite film as the immobilization matrix for colorectal cancer DNA sequence-selective electrochemical biosensor, Talanta 70 (2006) 561–565.

[17] X.L. Luo, J.J. Xu, J.L.Wang, H.Y. Chen, Electrochemically deposited nanocomposite of chitosan and carbon nanotubes for biosensor application, Chem. Commun. 2005, 2169-2171, DOI: 10.1039/B419197H.

[18] S.P. Singh, S.K. Arya, M.K. Pandey, B.D. Malhotra, S. Saha, K. Sreenivas, V. Gupta, Cholesterol biosensor based on rf sputtered zinc oxide nanoporous thin film, Appl. Phys. Lett. 91 (2007) 063901.

[19] A. Wei, X.W. Sun, J.X. Wang, Y. Lei, X.P. Cai, C.M. Li, Z.L. Dong, W. Huang, Enzymatic glucose biosensor based on ZnO nanorod arry grown by hydrothermal decomposition, Appl. Phys. Lett. 99 (2006) 123902.

[20] J.X. Wang, X.W. Sun, A. Wei, Y. Lei, X.P. Cai, C.M. Li, Z.L. Dong, Zinc oxide nanocomb biosensor for glucose detection, Appl. Phys. Lett. 88 (2006) 233106.

[21] A. Tiwari, SK. Shukla, Chitosan-g-polyaniline: a creatine amidinohydrolase immobilization matrix for creatine biosensor, Polym Lett. 3 (2009) 553-559.

[22] X.H. Xu, G.L. Re, J. Cheng, Q. Liu, D.G. Li, Q. Chen, Self-assembly of polyaniline-grafted chitosan/glucose oxidase nanolayered films for electrochemical biosensor applications, J Mater Sci 41 (2006) 4947-4977.

[23] A.G. Yavuz, A. Uygun, V.R. Bhethanabotla, Preparation of substituted polyaniline/chitosan composites by in situ electropolymerization and their application to glucose sensing, Carbohydrate Polym 81 (2010) 712-719.

[24] Y. Fang, Y. Ni, G. Zhang, C. Mao, X. Huang, J. Shen, Biocompatibility of CS–PPy nanocomposites and their application to glucose biosensor, Bioelectrochemistry 88 (2012) 1–7.

[25] A. Tiwari, S. Gong, Electrochemical detection of a breast cancer susceptible gene using cDNA immobilized chitosan-*co*-polyaniline electrode, Talanta 77 (2009) 1217-1222.

[26] S. Yadav, R. Devi, P. Bhar, S. Singhla, C.S. Pundir, Immobilization of creatininase, creatinase and sarcosine oxidase on iron oxide nanoparticles/chitosan-g-polyaniline modified Pt electrode for detection of creatinine, Enzym Microb Technol 50 (2012) 247–254.

[27] S. Yadava, R. Devia, A. Kumar, C.S. Pundir, Tri-enzyme functionalized ZnO-NPs/CHIT/c-MWCNT/PANI composite film for amperometric determination of creatinine, Biosens Bioelectron. 28 (2011) 64–70.

[28] K. Pandiselvi, S. Thambidurai, Chitosan-ZnO/polyaniline hybrid composites: Polymerization of aniline with chitosan-ZnO for better thermal and electrical property, Polym Degrad Stabil 98 (2013) 988-996.

[29] C.Y. Deng, J.H. Chen, Z. Nie, S.H. Si, A sensitive and stable biosensor based on the direct electrochemistry of glucose oxidase assembled layer-by-layer at the multiwall carbon nanotube-modified electrode, Biosens. Bioelectron. 26 (2010) 213-219.

[30] M.N. Zhang, K.P. Gong, H.W. Zhang, L.Q. Mao, Layer-by-layer assembled carbon nanotubes for selective determination of dopamine in the presence of ascorbic acid, Biosens. Bioelectron. 20 (2005) 1270-1276.

[31] M. Hojamberdiev, R.M. Prasad, K. Morita, M.A. Schiavon, R.Riedel, Polymer-derived mesoporous SiO2/ZnO nanocomposite for the purification of water contaminated with organic dyes, Microporous Mesoporous Mater 151 (2012) 330-338.

[32] C. Valls, P. Jimnez, E. Muoz, A.M. Benito, W.K. Maser, Simultaneous reduction of graphene oxide and polyaniline: doping-assited formation of a solid-state charge-transfer complex, J. Phys. Chem. C 115 (2011) 10468-10474.

[33] M. Cochet, G. Louarn, S. Quillard, J.P. Buisson, S. Lefrant, Theoretical and experimental vibrational study of polyaniline in base forms: non-planar analysis. Part I, J. Raman Spectrosc. 31 (2000) 1029–1039.

[34] A.V. Jadhav, C.G. Gulgas, A.D. Gudmundsdottir, Synthesis and properties of poly (aniline-co-azidoaniline). Eur Polym J 43 (2007) 2594-2603.

[35] K.A. Alim, V.A. Fonoberov, M. Shamsa, A.A. Balandin, Micro-Raman investigation of optical phonons in ZnO nanocrystals, J. Appl. Phys. 97 (2005) 124313-124317.

[36] G.K. Paul, A. Bhaumik, A.S. Patra, S.K. Bera, Enhanced photo-electric response of ZnO/polyaniline layer-by-layer self-assembled films. Mater Chem Phys 106 (2007) 360-363.

[37] S.A. Chen, L.C. Lin, Polyaniline doped by the new class of dopant, ionic salt: structure and properties. Macromolecules 28 (1995) 1239-1245.

[38] L. Brozova, P. Holler, J. Kovarova, J. Stejskal, M. Trchova, The stability of polyaniline in strongly alkaline or acidic aqueous media, Polym Degrad Stabil 93 (2008) 592-600.

[39] M. Andrés-Vergés, C.J. Serna, Morphological characterization of ZnO powders by X-ray and IR spectroscopy. J Mater Sci Lett 7 (1988) 970-972.

[40] H. Zhong, R. Yuan, Y. Chai, W. Li, X. Zhong, Y. Zhang, In situ chemo-synthesized multi-wall carbon nanotube-conductive polyaniline nanocomposites: Characterization and application for a glucose amperometric biosensor, Talanta 1 (2011) 104-111.

[41] Y.Y. Liang, L.M. Zhang, W. Li, R.F. Chen, Polysaccharide-modified iron oxide nanoparticles as an effective magnetic affinity adsorbent for bovine serum albumin. Colloid Polym Sci 285 (2007)1193-1199.

[42] H. Peng, G. Ma, W. Ying, A. Wang, H. Huang, Z, Lei, In situ synthesis of polyaniline/sodium carboxymethyl cellulose nanorods for high-performance redox supercapacitors, J. Power Sources 211 (2012) 40-45.

[43] M. Sharp, M. Petersson, K. Edstrom, Preliminary determinations of electron transfer kinetics involving ferrocene covalently attached to a platinum surface, J. Electroanal. Chem. 95 (1979) 123–130.

[44] Y. Liu, X. Qu, H. Guo, H. Chen, B. Liu, S. Dong, Facile preparation of amperometric laccase biosensor with multifunction based on the matrix of carbon nanotubes–chitosan composite, Biosens. Bioelectron. 21 (2006) 2195–2201.

[45] D. Zheng, J. Ye, L. Zhou, Y. Zhang, C. Yu, Simultaneous determination of dopamine, ascorbic acid and uric acid on ordered mesoporous carbon/Nafion composite film, J. Electroanal. Chem. 625 (2009) 82–87.

[46] F. Malem, D. Mandler, Self-assembled monolayers in electroanalytical chemistry: application of ω-mercapto carboxylic acid monolayers for the electrochemical detection of dopamine in the presence of a high concentration of ascorbic acid, Anal. Chem. 65 (1993) 37–41.

[47] C.R. Raj, K. Tokuda, T. Ohsaka, Electroanalytical applications of cationic self-assembled monolayers: square-wave voltammetric determination of dopamine and ascorbate, Bioelectrochemistry 53 (2001) 183–191.

[48] M.J. Giz, B. Duong, N.J. Tao, In situ STM study of self-assembled mercaptopropionic acid monolayers for electrochemical detection of dopamine, J. Electroanal. Chem. 465 (1999) 72–79.

[49] L. Yang, S. Liu, Q. Zhang, F. Li, Simultaneous electrochemical determination of dopamine and ascorbic acid using AuNPs@polyaniline core–shell nanocomposites modified electrode, Talanta 89 (2012) 136– 141.

[50] Z. Jia, J. Liu, Y.B. Shen, Fabrication of a template-synthesized gold nanorod-modified electrode for the detection of dopamine in the presence of ascorbic acid, Electrochem. Commun. 9 (2007) 2739–2743.

[51] K. Wu, J. Fei, S. Hu, Simultaneous determination of dopamine and serotonin on a glassy carbon electrode coated with a film of carbon nanotubes, Anal. Biochem. 318 (2003) 100–106.

[52] L. Zhang, X.Q. Lin, Electrochemical behavior of a covalently modified glassy carbon electrode with aspartic acid and its use for voltammetric differentiation of dopamine and ascorbic acid, Anal. Bioanal. Chem. 382 (2005) 1669-1677.

[53] Y.F. Zhao, Y.Q. Gao, D.P. Zhan, H. Liu, Q. Zhao, Y. Kou, Y.H. Shao, M.X. Li, Q.K. Zhuang, Z.W. Zhu, Selective detection of dopamine in the presence of ascorbic acid and uric acid by a carbon nanotubes-ionic liquid gel modified electrode, Talanta 66 (2005) 51–57.

[54] C. Xia, C. Xiaolan, W. Ning, Selective sensing of dopamine at MnOOH nanobelt modified electrode, Sens. Actuators B: Chem. 160 (2011) 771– 776.

[55] C.F. Tang, S. Ashok kumar, S.M. Chen, Zinc oxide/redox mediator composite films-based sensor for electrochemical detection of important biomolecules, Anal. Biochem. 380 (2008) 174–183.

[56] N.Q. Jia, Z.Y. Wang, G.F. Yang, H.B. Shen, L.Z. Zhu, Electrochemical properties of ordered mesoporous carbon and its electroanalytical application for selective determination of dopamine, Electrochem. Commun.9 (2007) 233–238.

[57] R.G.A. Bone, H.O. Villar, Discriminating D1 and D2 agonists with a hydrophobic similarity index, J. Mol. Graph. 13 (1995) 201-208.

[58] IUPAC, Recommendations for the definition, estimation and use of the detection limit, Analyst 112 (1987) 199-204.

[59] Y.R. Kim, S. Bong, Y.J. Kang, Y. Yang, R.K. Mahajan, J.S. Kim, H. Kim, Electrochemical detection of dopamine in the presence of ascorbic acid using graphene modified electrodes, Biosens. Bioelectron. 25 (2010) 2366–2369.

[60] Y. Fan, H.T. Lu, J.H. Liu, C.P. Yang, Q.S. Jing, Y.X. Zhang, X.K. Yang, K.J. Huang, Hydrothermal preparation and electrochemical sensing properties of TiO_2–graphene nanocomposite, Colloids and Surfaces B 83 (2011) 78-82.

[61] A.S. Adekunle, B.O. Agboola, J. Pillay, K.I. Ozoemena, Electrocatalytic detection of dopamine at single-walled carbon nanotubes-iron(III) oxide nanoparticles platform, Sens. Actuators B: Chem. 148 (2010) 93-102.

[62] S. Lupu, F.J.D. Campo, F.X. Munoz, Development of microelectrode arrays modified with inorganic–organic composite materials for dopamine electroanalysis, Electroanal Chem. 639 (2010) 147–153.

[63] W. Yan, X. Feng, X. Chen, X. Li, J.J. Zhu, A selective dopamine biosensor based on AgCl@polyaniline core–shell nanocomposites, Bioelectrochemistry 72 (2008) 21–27.

[64] Z.C. Chen, C. Fang, G.Z. Qw, J.S. He, Z.S. Deng, Non-enzymatic disposable test strip for detecting uric acid in whole blood, Electroanal Chem. 633 (2009) 314–318.

Figure captions

Fig. 1. SEM images of CS-PANI (a), CS-$ZC_{2.5}$/PANI (b), CS-ZC_5/PANI (c) and $CS_{0.12}$-$ZC_{2.5}$/PANI (d) modified electrodes.

Fig. 2. TEM images of CS-PANI (a), CS-$ZC_{2.5}$/PANI (b), CS-ZC_5/PANI (c) and $CS_{0.12}$-$ZC_{2.5}$/PANI modified electrodes. Inset (d): SEAD pattern of $CS_{0.12}$-$ZC_{2.5}$/PANI.

Fig. 3. (A) Raman and (B) FTIR spectra of CS-PANI and $CS_{0.12}$-$ZC_{2.5}$/PANI nanocomposites modified electrodes.

Fig. 4. Cyclic voltammograms of bare GCE (a), CS-PANI (b), CS-$ZC_{2.5}$/PANI (c), CS-ZC_5/PANI (d) and $CS_{0.12}$-$ZC_{2.5}$/PANI (e) in pH 7.0 PBS solution containing 1 mM $[Fe(CN)_6]^{3-/4-}$; scan rate: 50 mVs^{-1}.

Fig. 5. Cyclic voltammograms of $CS_{0.12}$-$ZC_{2.5}$/PANI modified GCE in pH 7.0 PBS solution containing 1 mM $[Fe(CN)_6]^{3-/4-}$ under different scan rates (from inner to outer): 50, 100, 150, 200, 250, 300, 350, 400, 450, 500, 550 and 600 mV s^{-1}; Inset: plots for corresponding anodic and cathodic peak current against scan rate.

Fig. 6. Electrochemical impedance spectroscopy for bare GCE (a), CS-PANI (b) and $CS_{0.12}$-$ZC_{2.5}$/PANI/GCE in pH 7.0 PBS solution containing 1 mM $[Fe(CN)_6]^{3-/4-}$.

Fig. 7. (A) Cyclic voltammograms of the (a) bare GCE in pH 7.0 PBS (b) bare GCE and (c) $CS_{0.12}$-$ZC_{2.5}$/PANI modified GCE in pH 7.0 PBS solution containing 0.5 mM AsA. (B) $CS_{0.12}$-$ZC_{2.5}$/PANI modified GCE different concentrations of AsA: (i) 1 mM, (ii) 2 mM, (iii) 3 mM, (iv) 4 mM and (v) 5 mM in pH 7.0 PBS (); scan rate = 50 mV/s.

Fig. 8. (A) Cyclic voltammograms of the (a) bare GCE and (b) $CS_{0.12}$- $ZC_{2.5}$/PANI modified GCE in pH 7.0 PBS solutions containing 0.1 mM DA. (B) $CS_{0.12}$-$ZC_{2.5}$/PANI modified GCE with different concentrations of DA: (i) 0.1 mM, (ii) 0.2 mM,(iii) 0.3 mM, (iv) 0.4 mM and (v) 0.5 mM in pH 7.0 PBS; scan rate = 50 mV/s.

Fig. 9. Cyclic voltammograms of (a) bare GCE and (b) $CS_{0.12}$-$ZC_{2.5}$/PANI modified GCE in pH 7.0 PBS containing 1 mM AsA and DA at a scan rate of 50 mV s^{-1}.

Fig. 10. (A) Differential pulse voltammograms of 1 mM AsA and 0.1 mM DA in pH 7.0 PBS at (a) bare GCE and (b) $CS_{0.12}$-$ZC_{2.5}$/PANI/GCE. (B) DPVs of DA in the presence of 140 μM AsA, recorded using the $CS_{0.12}$-$ZC_{2.5}$/PANI/GCE in pH 7.0 PBS. DA concentration (from i-ix): 20 x 10^{-5}, 40 x 10^{-5}, 60 x 10^{-5}, 80 x 10^{-5}, 100 x 10^{-5}, 120 x 10^{-5}, 140 x 10^{-5}, 160 x 10^{-5} and 180 x 10^{-5} mol dm^{-3}. Inset: the linear regression curve of peak current vs. DA concentration.

Fig. 11. Differential pulse voltammograms in pH 7 PBS containing 0.1 mM AsA, glucose and different concentration range of DA: (a-d = 0.001-0.005 mM) at the $CS_{0.12}$-$C_{2.5}$/PANI/GCE.

Scheme. 1. Schematic illustration of the catalysis of DA.

Captions for Tables

Table 1: Comparison of different modified electrodes for dopamine detection.

Table 2: Determination of dopamine content in dopamine hydrochloride injections.

Table 1

Comparison of different modified electrodes for dopamine detection.

Modifier	Method	Linear range (μ M)	Detection limit (μ M)	Ref
Graphene modified GCE	DPV[a]	4-100	2.64	[59]
TiO_2-graphene modified GCE	DPV[a]	5-200	2.0	[60]
SWCNT/Fe_2O_3modified graphite electrode	SWV[b]	3.2-31.8	0.36	[61]
Inorganic-organic composite	CV[c]	10-50	4.3	[62]
Nafion-AgCl@PANI modified GC electrode	SW[b]	0.2-8.0	0.49	[63]
CS-ZnO/PANI modified GC electrode	**DPV[a]**	**20-180**	**0.21**	**This work**

[a] differential pulse voltammetry

[b] square wave voltammetry

[c] cyclic voltammetry

Table 2

Determination of dopamine content in dopamine hydrochloride injections.

Sample	DA added (μM)	DA found (μM)	R.S.D (%)	Recovery (%)
1	4.3	4.02± 0.0007	2.71	98.67
2	6.4	6.23± 0.0015	3.01	97.72
3	8.5	8.35± 0.0024	3.52	98.45

Highlights

- Glassy carbon electrode was modified with chitosan-ZnO/polyaniline film
- Dopamine was detected by electrochemically in presence of ascorbic acid at pH 7.0.
- It is a stable and reproducible sensor without using any specific reagent.
- The resultant sensor possesses high sensitivity and good selectivity.

Figure(s)

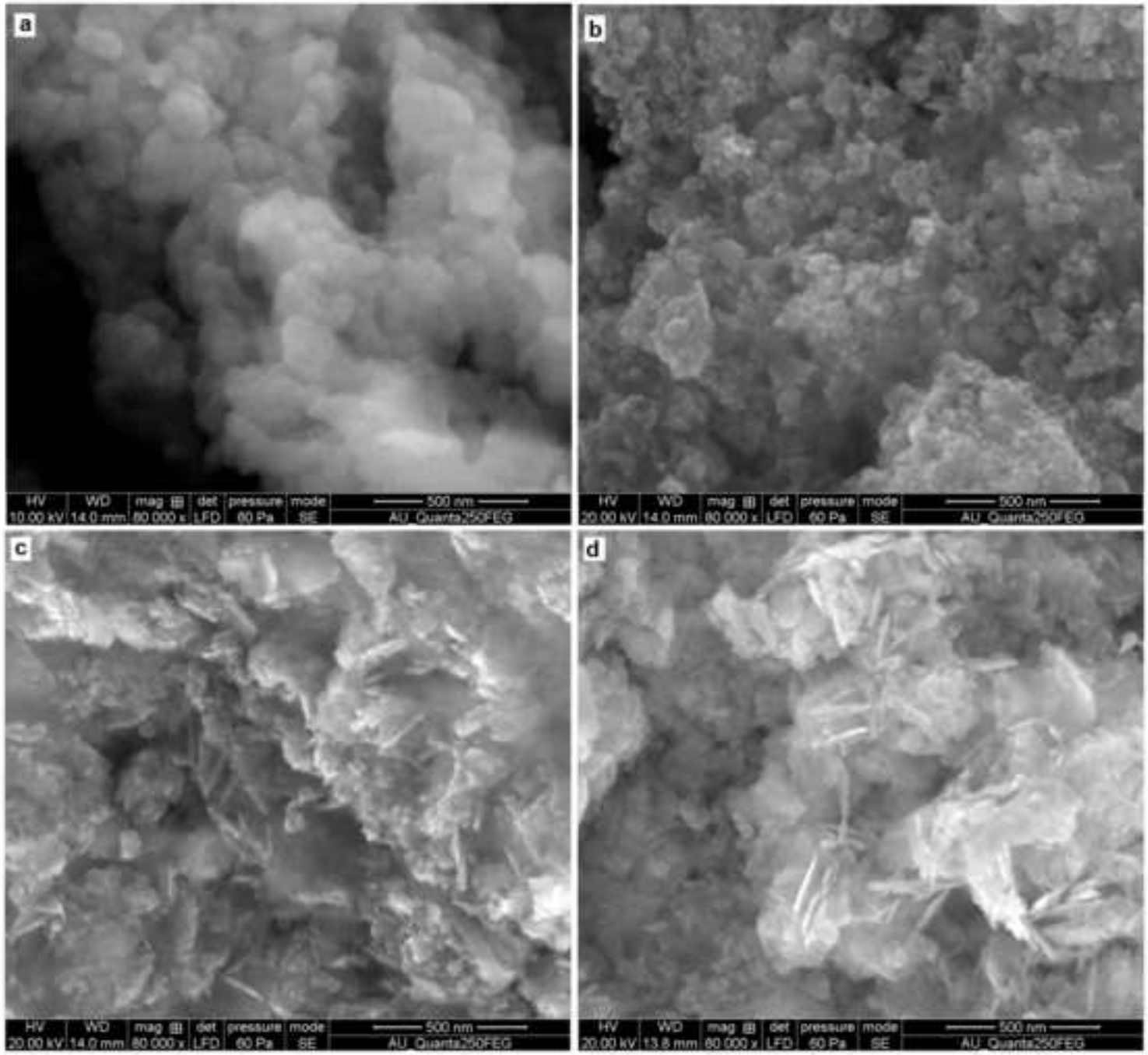

Fig. 1. SEM images of CS-PANI (a), CS-$ZC_{2.5}$/PANI (b), CS-ZC_5/PANI (c) and $CS_{0.12}$-$ZC_{2.5}$/PANI (d) modified electrodes.

Figure(s)

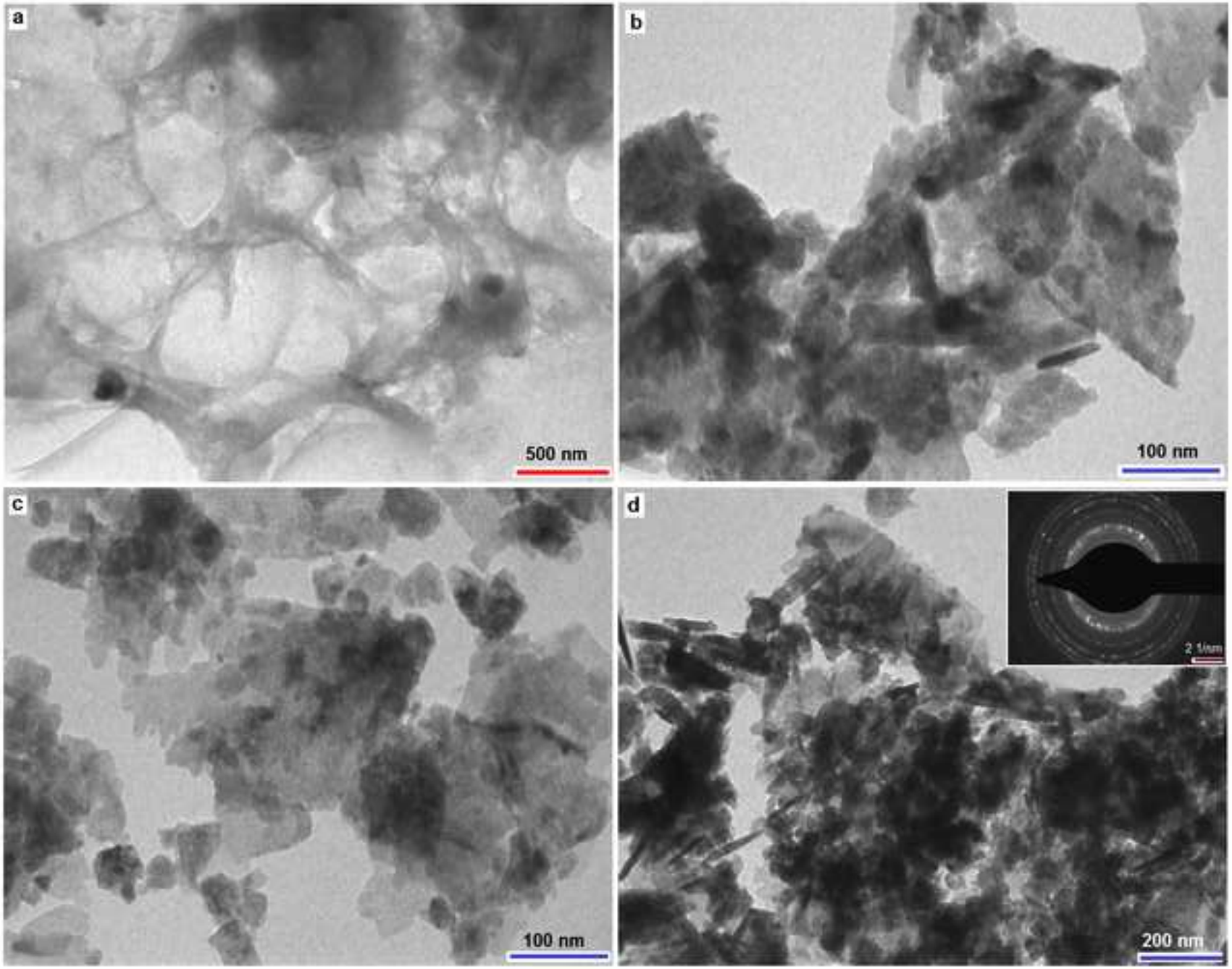

Fig. 2. TEM images of CS-PANI (a), CS-$ZC_{2.5}$/PANI (b), CS-ZC_5/PANI (c) and $CS_{0.12}$-$ZC_{2.5}$/PANI (d) modified electrodes. inset (d): SAED pattern of $CS_{0.12}$-$ZC_{2.5}$/PANI.

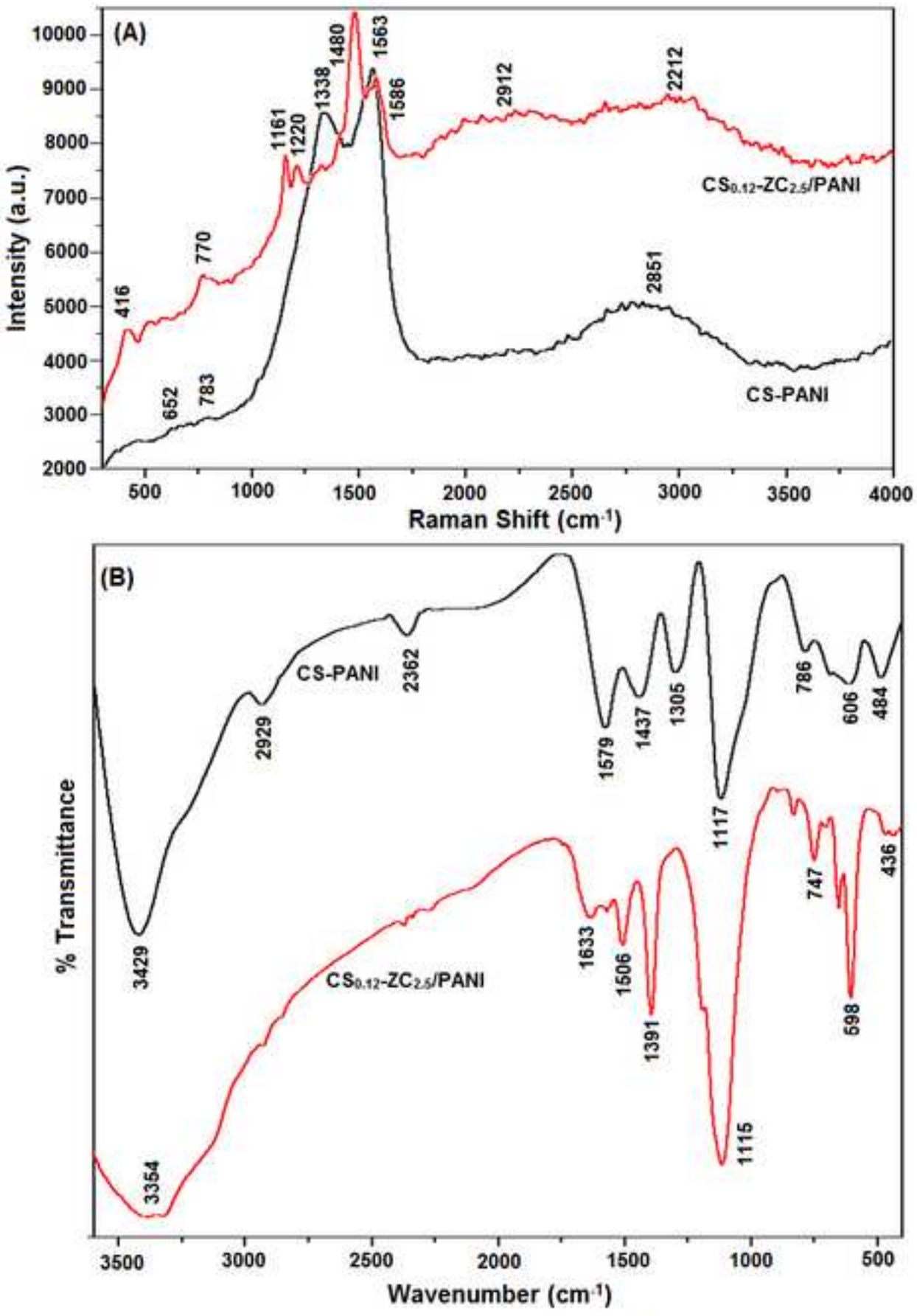

Fig. 3. (A) Raman and (B) FTIR spectra of CS-PANI and $CS_{0.12}$-$ZC_{2.5}$/PANI nanocomposites modified electrodes.

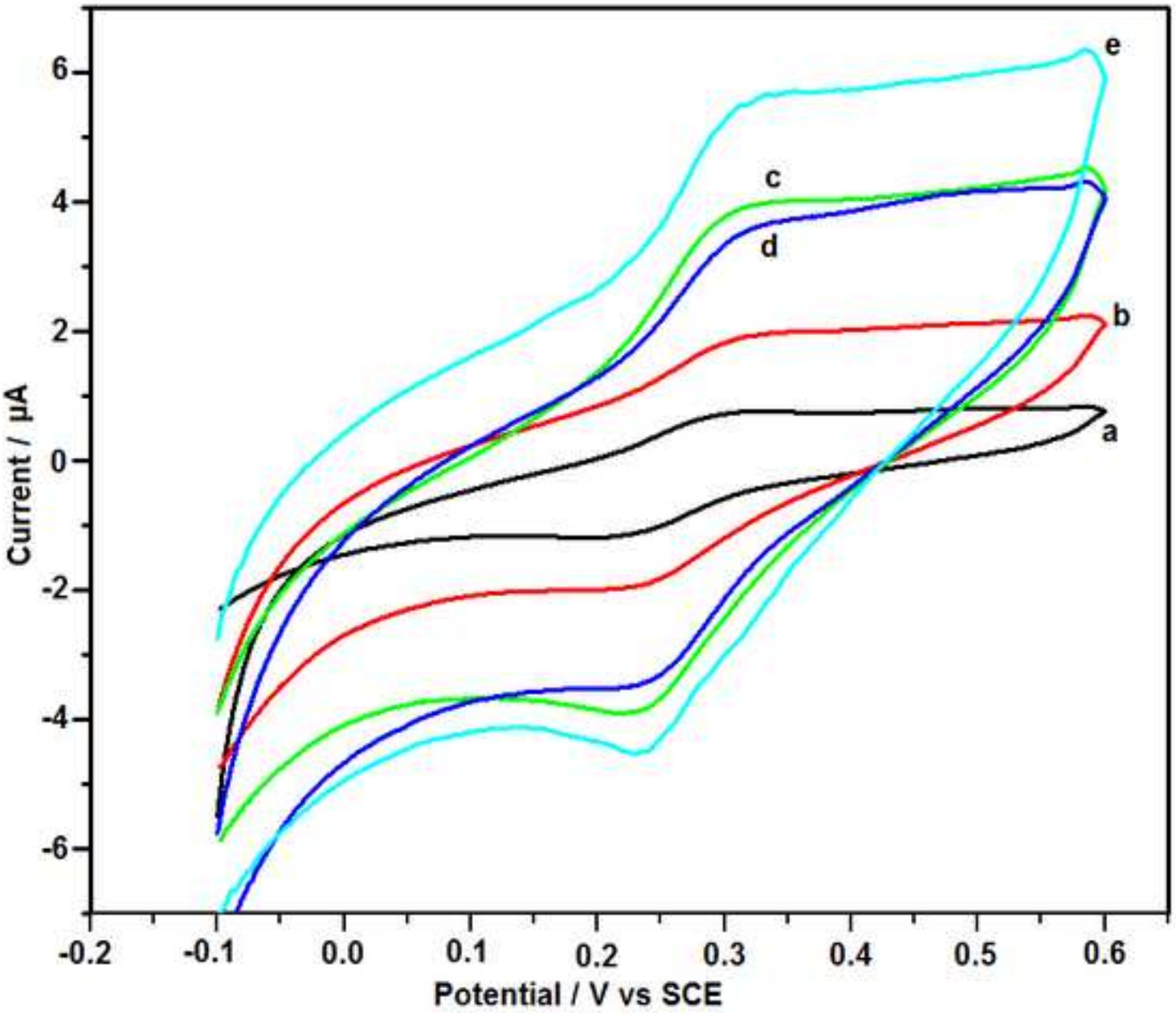

Fig. 4. Cyclic voltammograms of bare GCE (a), CS-PANI (b) CS-$ZC_{2.5}$/PANI (c), CS-ZC_5/PANI (d) and $CS_{0.12}$-$ZC_{2.5}$/PANI (e) in pH 7.0 PBS solution containing 1 mM $[Fe(CN)_6]^{3-/4-}$; scan rate: 50 mVs^{-1}.

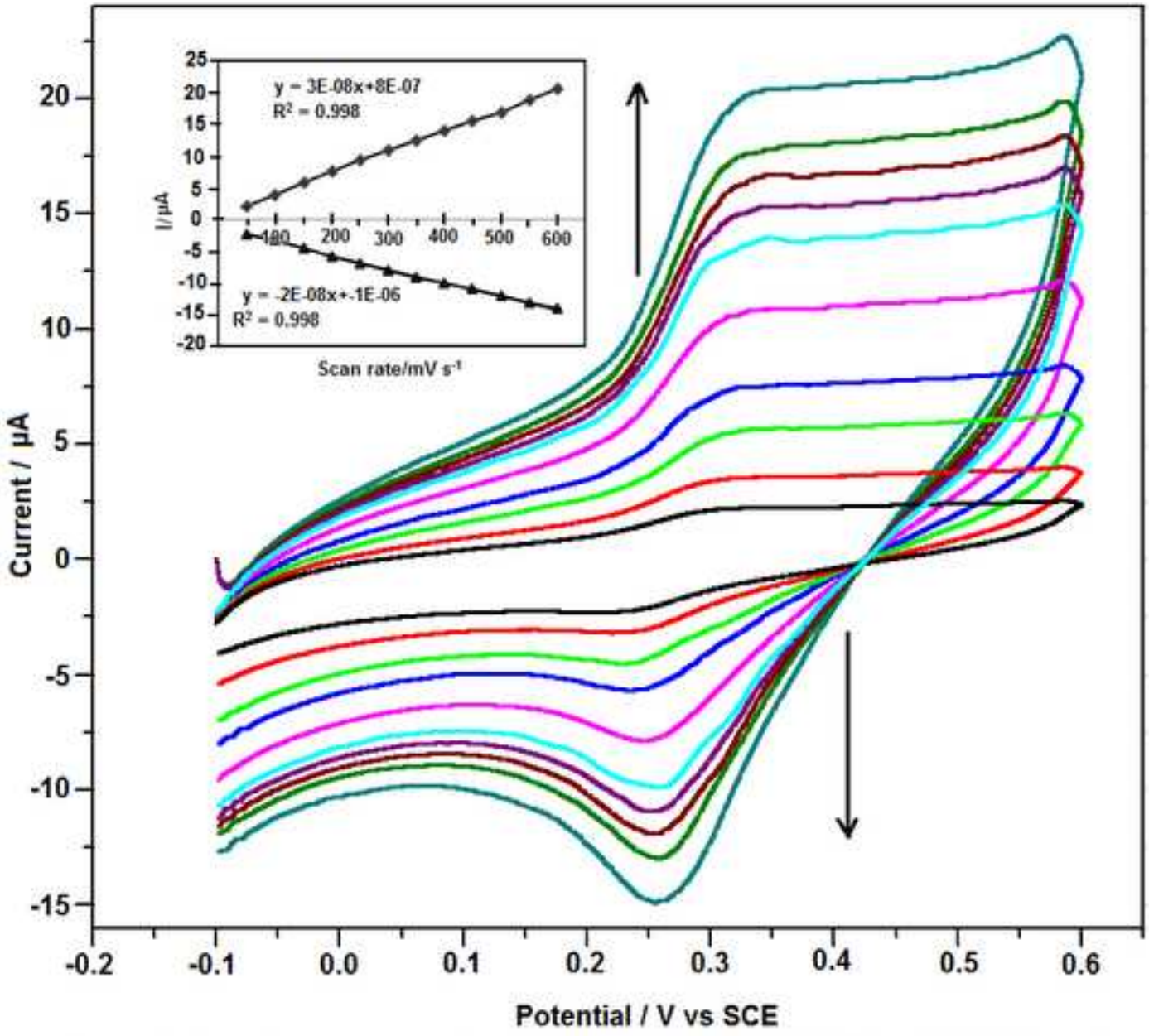

Fig. 5. Cyclic voltammograms of $CS_{0.12}$-$ZC_{2.5}$/PANI modified GCE in pH 7.0 PBS solution containing 1 mM $[Fe(CN)_6]^{3-/4-}$ under different scan rates (from inner to outer): 50, 100, 150, 200, 250, 300, 350, 400, 450, 500, 550 and 600 mV s^{-1}; Inset: plots for corresponding anodic and cathodic peak current against scan rate.

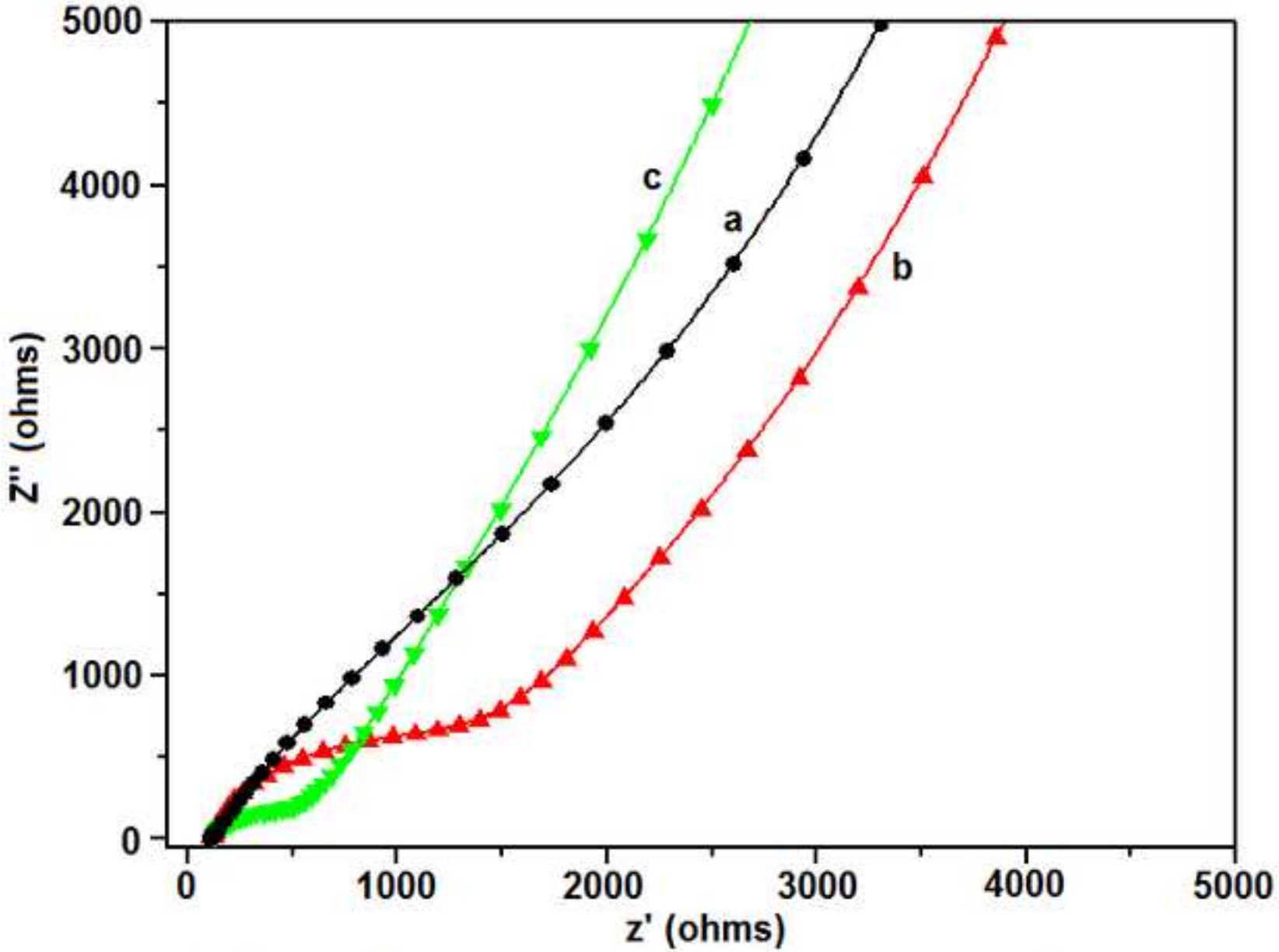

Fig. 6. Electrochemical impedance spectroscopy for bare GCE (a), CS-PANI (b) and $CS_{0.12}$-$ZC_{2.5}$/PANI/GCE in pH 7.0 PBS solution containing 1 mM $[Fe(CN)_6]^{3-/4-}$.

Figure(s)

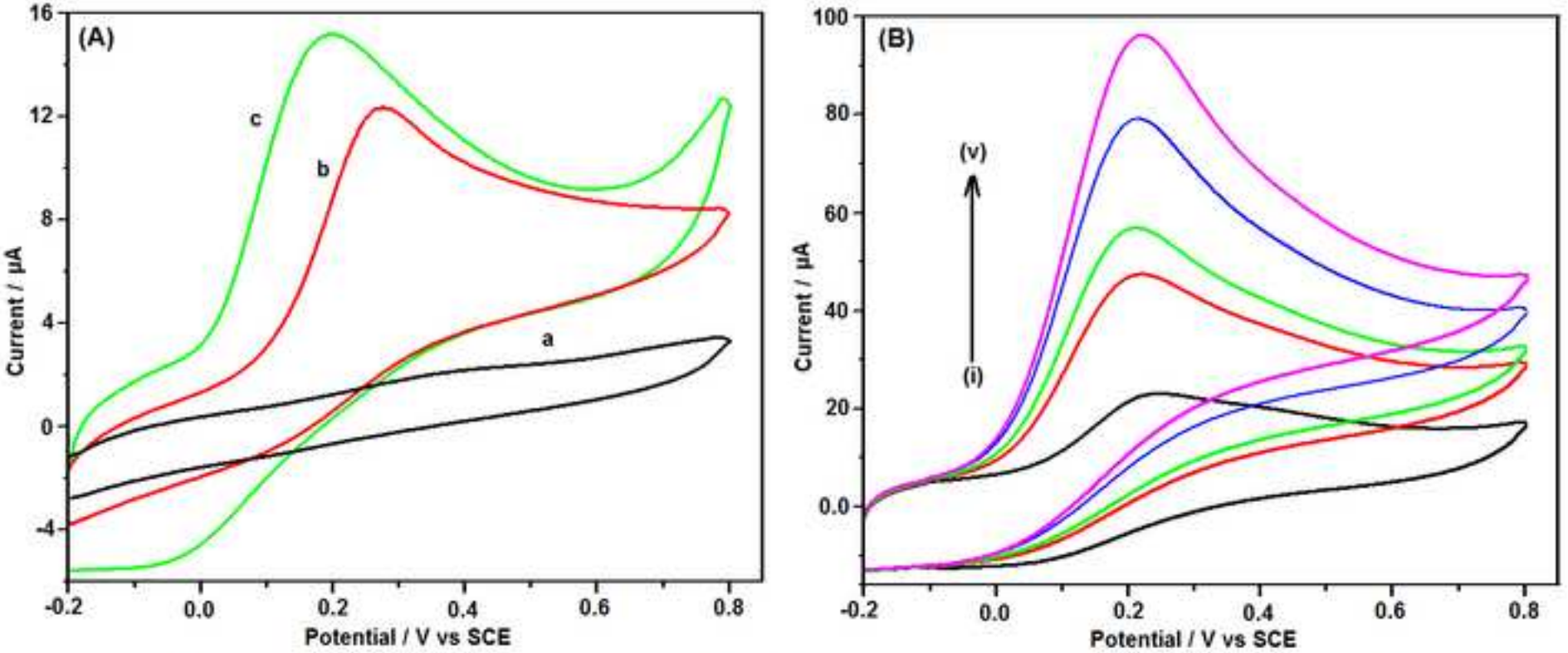

Fig. 7. (A) Cyclic voltammograms of the (a) bare GCE in pH 7.0 PBS (b) bare GCE and (c) $CS_{0.12}$-$ZC_{2.5}$/PANI modified GCE in pH 7.0 PBS solution containing 0.5 mM AsA. (B) $CS_{0.12}$-$ZC_{2.5}$/PANI modified GCE different concentrations of AsA : (i) 1 mM, (ii) 2mM, (iii) 3 mM, (iv) 4 mM and (v) 5 mM in pH 7.0 PBS ; scan rate = 50 mV/s.

Figure(s)

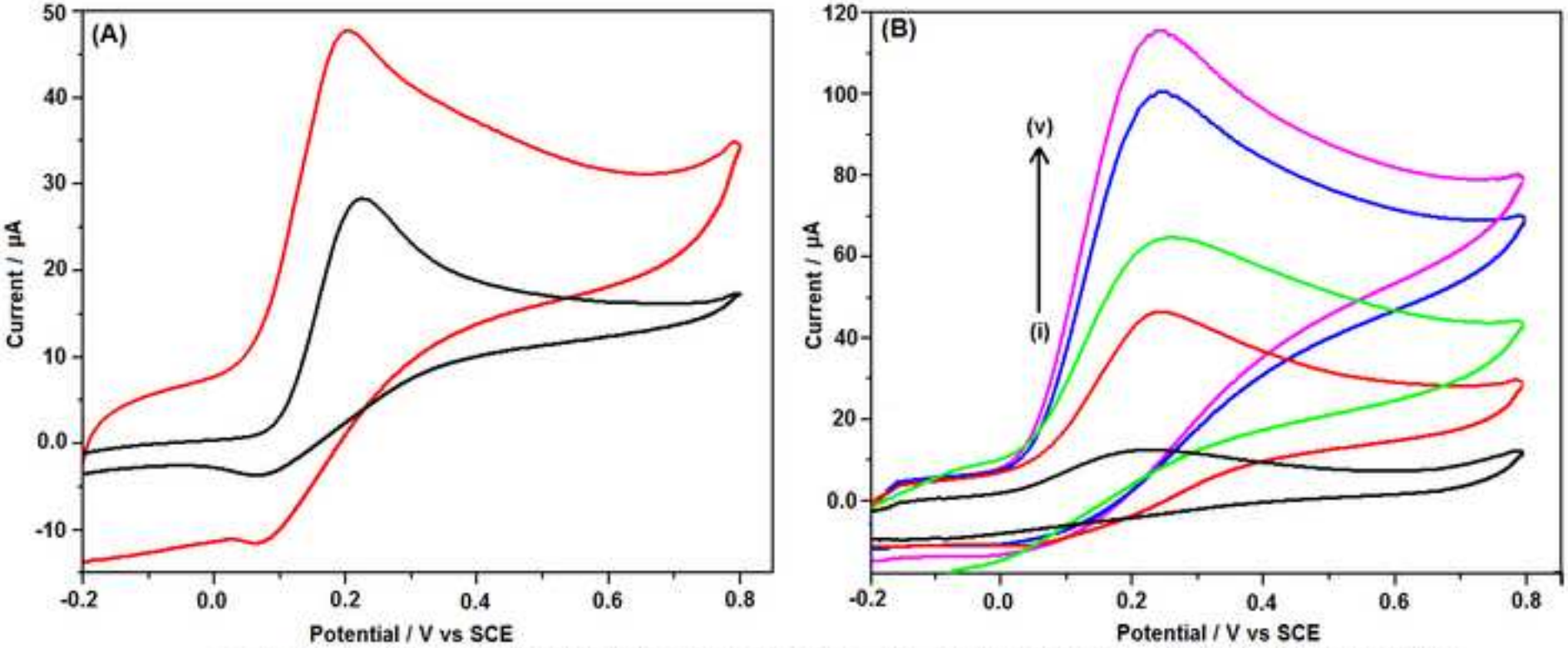

Fig. 8. (A) Cyclic voltammograms of the (a) bare GCE and (b) $CS_{0.12}$-$ZC_{2.5}$/PANI modified GCE in pH 7.0 PBS solutions containing 0.1 mM DA. (B) $CS_{0.12}$-$ZC_{2.5}$/PANI modified GCE with different concentrations of DA: (i) 0.1 mM, (ii) 0.2 mM, (iii) 0.3 mM, (iv) 0.4 mM and (v) 0.5 mM in pH 7.0 PBS; scan rate = 50 mV/s.

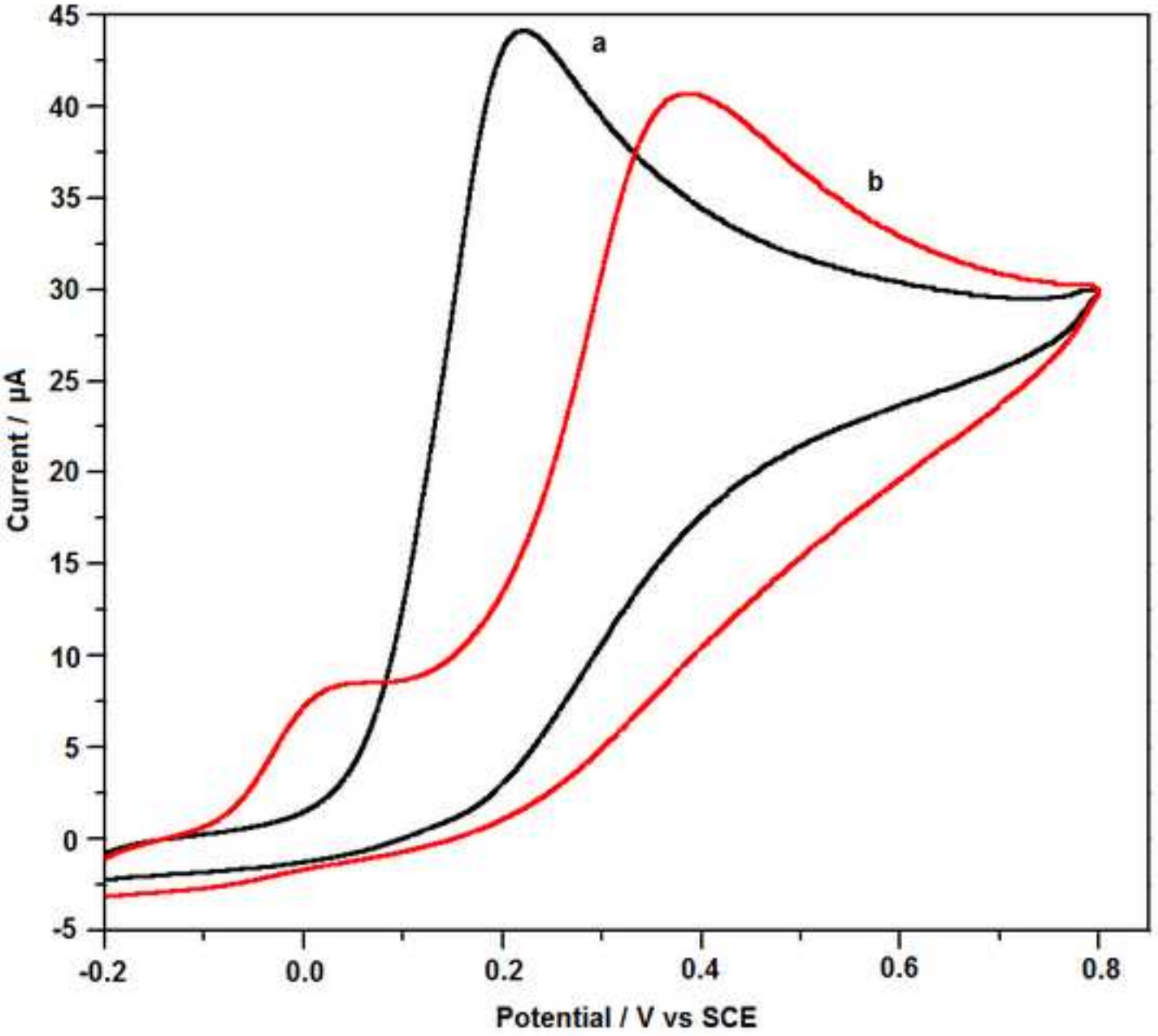

Fig. 9. Cyclic voltammograms of (a) bare GCE and (b) $CS_{0.12}$-$ZC_{2.5}$/PANI modified GCE in pH 7.0 PBS containing 1 mM AsA and DA at a scan rate of 50 mV s^{-1}.

Figure(s)

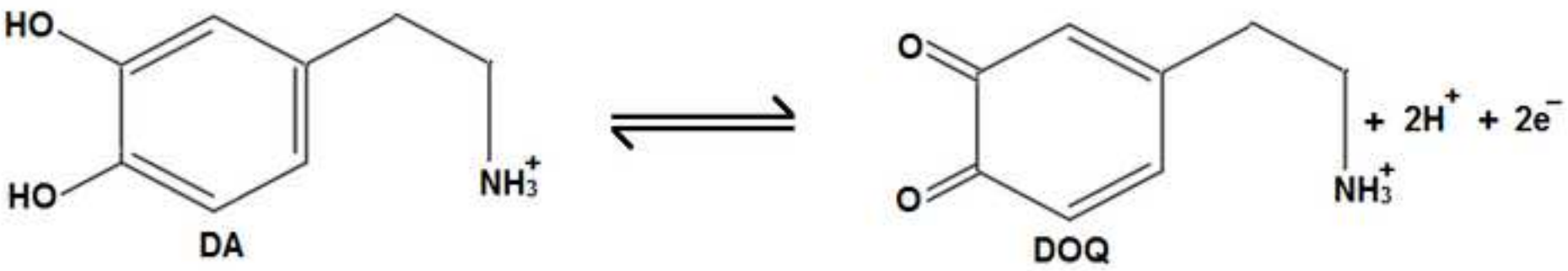

Scheme. 1. Schematic illustration of the catalysis of DA.

Figure(s)

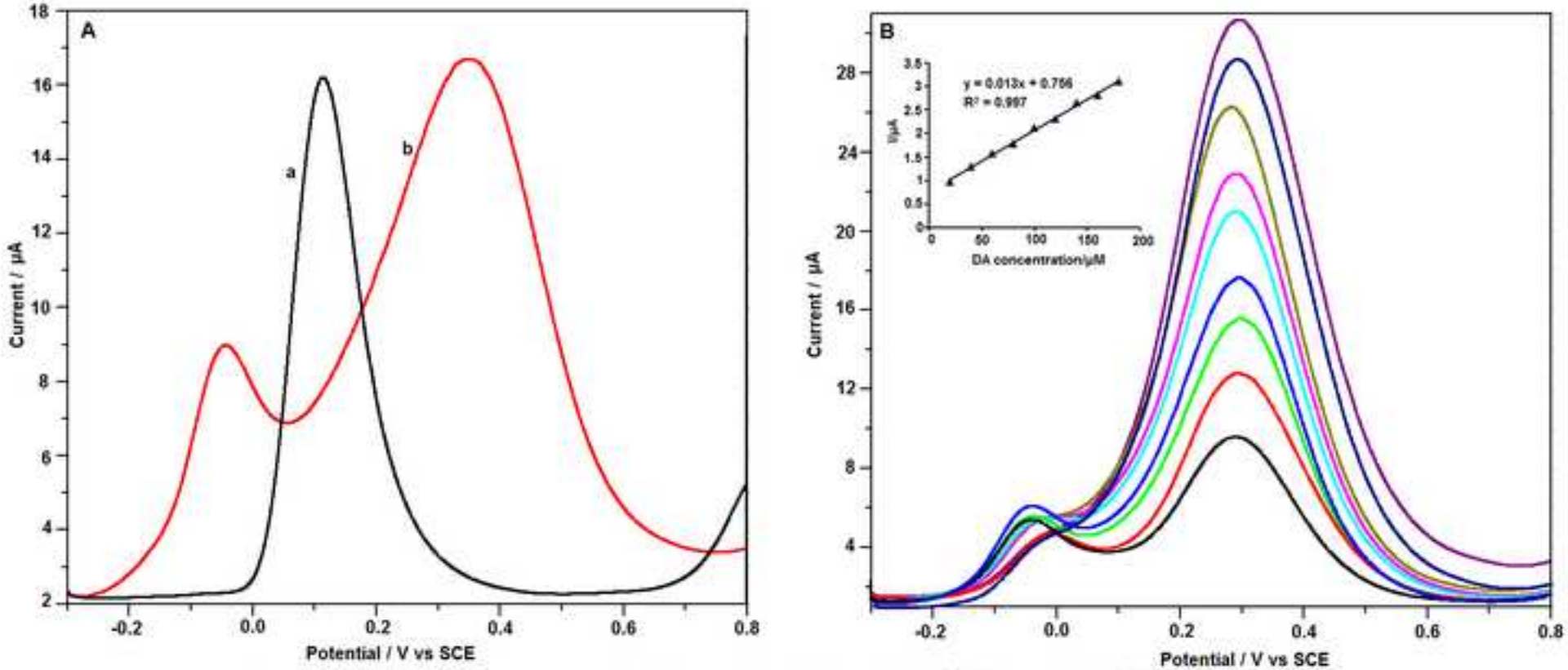

Fig.10. (A) Differential pulse voltammograms of 1mM AsA and 0.1 mM DA in pH 7.0 PBS at (a) bare GCE and (b) $CS_{0.12}$-$ZC_{2.5}$/PANI/GCE. (B) DPVs of DA in the presence of 140 µM AsA, recorded using the $CS_{0.12}$-$ZC_{2.5}$/PANI/GCE in pH 7.0 PBS DA concentration (from i-ix): 20 x 10^{-5}, 40 x 10^{-5}, 60 x 10^{-5}, 80 x 10^{-5}, 100 x 10^{-5}, 120 x 10^{-5}, 140 x 10^{-5}, 160 x 10^{-5} and 180 x 10^{-5} mol dm^{-3}. Inset: the linear regression curve of peak current vs. DA concentration.

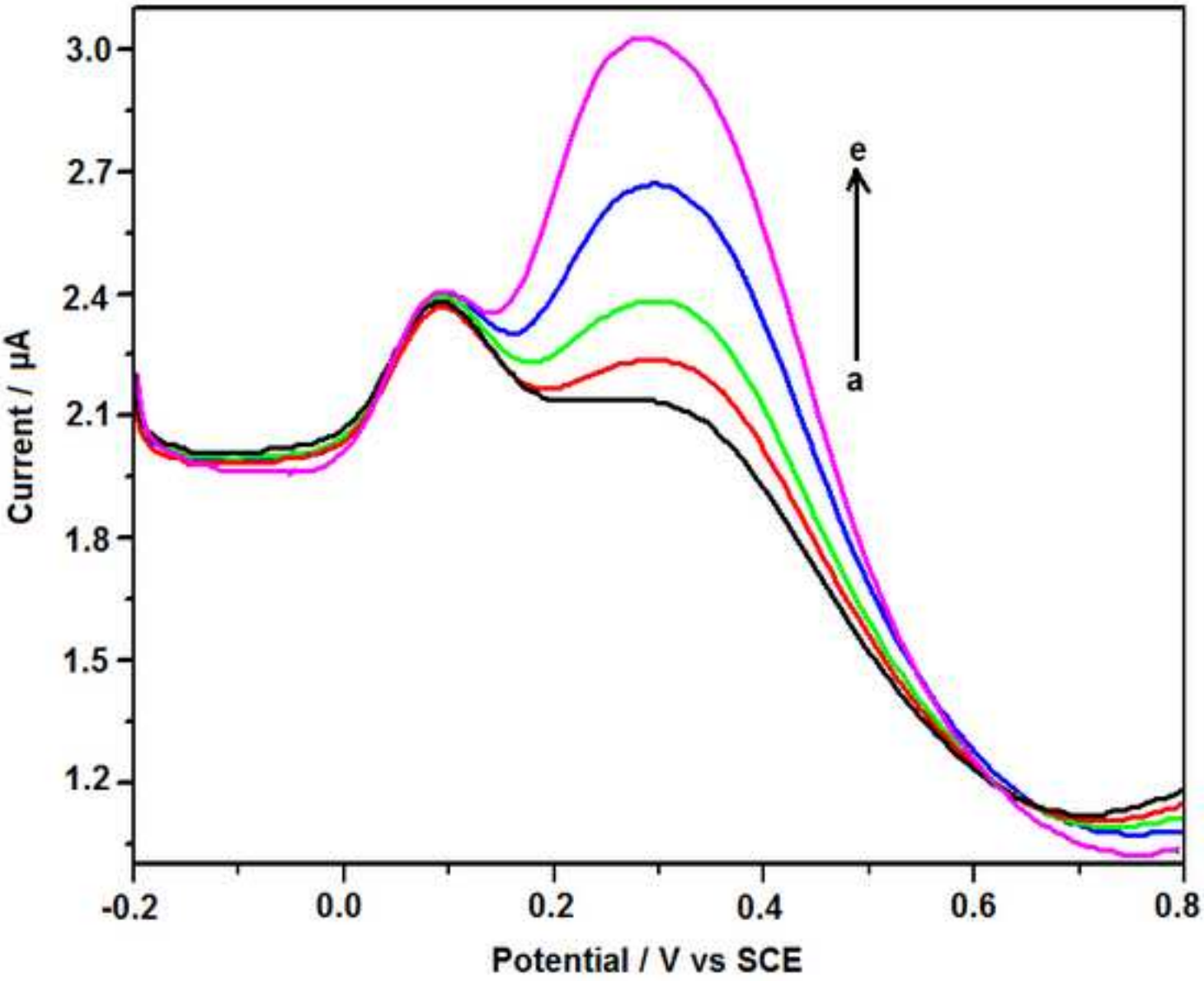

Fig. 11 . Differential pulse voltammograms in pH 7.0 PBS containing 0.1mM AsA, glucose and different concentration range of DA: (a-d = 0.001-0.005 mM) at the $CS_{0.12}$-$ZC_{2.5}$/PANI/GCE.